JOURNAL OF ENZYME INHIBITION AND MEDICINAL CHEMISTRY
2025, VOL. 40, NO. 1, 2447719
https://doi.org/10.1080/14756366.2024.2447719

Taylor & Francis
Taylor & Francis Group

RESEARCH ARTICLE

OPEN ACCESS Check for updates

Indirubin-3′-oxime as a dual-action agent: mitigating heat-induced male infertility in *Drosophila melanogaster* and inhibiting soluble epoxide hydrolase

Nguyen Viet Phong[a‡], Hyo-Sung Kim[b,c,d‡], Yan Zhao[e], Eunbyul Yeom[b,c,d] and Seo Young Yang[a]

[a]Department of Biology Education, Teachers College and Institute for Phylogenomics and Evolution, Kyungpook National University, Daegu, Republic of Korea; [b]School of Life Science and Biotechnology, College of Natural Sciences, Kyungpook National University, Daegu, Republic of Korea; [c]School of Life Sciences, BK21 FOUR KNU Creative BioResearch Group, Kyungpook National University, Daegu, Republic of Korea; [d]School of Life Sciences, College of Natural Sciences, KNU-G LAMP Project Group, KNU-Institute of Basic Sciences, Kyungpook National University, Daegu, Republic of Korea; [e]School of Pharmacy, Yantai University, Yantai, PR China

ABSTRACT

This study investigated the potential of the indirubin-3′-oxime (I3O) compound to mitigate temperature-induced male infertility in *Drosophila melanogaster*. Elevated temperatures significantly reduced egg-hatching rates, but I3O supplementation improved these rates, suggesting it can partially restore fertility under heat stress. Additionally, I3O was found to inhibit soluble epoxide hydrolase (sEH), an enzyme involved in the metabolism of epoxyeicosatrienoic acids, which are vital for reproductive health. I3O exhibited sEH inhibitions with an IC_{50} value of 59.74 ± 0.41 μM. Enzyme kinetics revealed that I3O acts as a non-competitive inhibitor of sEH with a K_i value of 78.88 μM. Molecular docking showed strong interactions between I3O and key residues in the allosteric regions within the sEH enzyme, with a binding affinity of −9.2 kcal/mol. These interactions were supported by 100 ns molecular dynamics simulations, which confirmed the stability of the sEH–I3O complex.

GRAPHICAL ABSTRACT

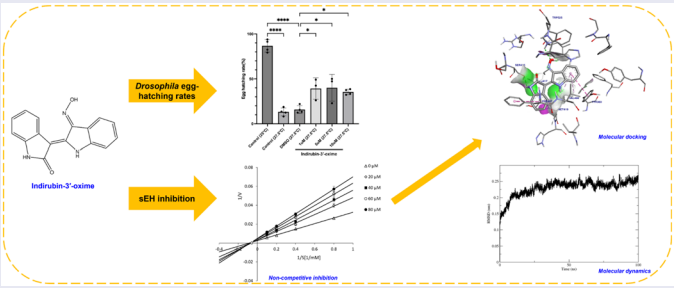

ARTICLE HISTORY
Received 4 September 2024
Revised 29 November 2024
Accepted 23 December 2024

KEYWORDS
Indirubin-3′-oxime; male infertility; *Drosophila melanogaster*; soluble epoxide hydrolase; molecular dynamics

Introduction

Male infertility is an increasingly prevalent issue that is exacerbated by environmental stressors, such as elevated temperatures, which can adversely affect reproductive health[1–3]. In *Drosophila melanogaster*, a well-established model organism, heat stress significantly reduces egg-hatching rates, a key indicator of male fertility[4–7]. The underlying mechanisms contributing to temperature-induced infertility are complex and multifaceted, involving factors such as inflammation, oxidative stress, and vascular dysfunction[2,8].

Soluble epoxide hydrolase (sEH) is a critical enzyme involved in the metabolism of epoxyeicosatrienoic acids (EETs)[9,10], signalling molecules that play significant roles in various physiological processes, including inflammation, oxidative stress, and vascular function[11]. EETs are known for their anti-inflammatory and antioxidative properties, which are essential for maintaining overall health, including reproductive health[12,13]. Elevated sEH activity can reduce EET levels, leading to increased inflammation and oxidative stress, both of which are detrimental to reproductive health. Moreover, EETs are crucial for maintaining optimal vascular function, which is essential for regulating sufficient blood flow to reproductive organs[14,15]. Therefore, inhibiting sEH to preserve EET levels could mitigate these negative effects, potentially offering therapeutic benefits in managing conditions associated with male infertility.

Indirubin-3′-oxime (I3O), a derivative of indirubin, is a bioactive compound traditionally recognised in Chinese medicine for its therapeutic role in treating chronic diseases, including

CONTACT Eunbyul Yeom yeb@knu.ac.kr School of Life Science and Biotechnology, College of Natural Sciences, Kyungpook National University, Daegu 41566, Republic of Korea; Seo Young Yang syy@knu.ac.kr Department of Biology Education, Teachers College and Institute for Phylogenomics and Evolution, Kyungpook National University, Daegu 41566, Republic of Korea
‡Both authors contributed equally to this work.

leukaemia and inflammatory conditions[16–18]. Recently, I3O has attracted significant attention for its wide range of pharmacological activities. Indeed, it exhibits potent anti-inflammatory effects, primarily by inhibiting key signalling pathways such as glycogen synthase kinase-3β (GSK-3β) and cyclin-dependent kinases (CDKs), which are critical in cell proliferation, apoptosis, and inflammation[18,19]. Moreover, I3O has been shown to modulate immune responses and suppress tumour growth in various cancer cell lines by inducing cell cycle arrest and promoting apoptosis in various cancer cell lines[20–22]. The neuroprotective effects of I3O are also noteworthy, as the compound demonstrates a potential to protect neurons from oxidative stress and inflammatory damage, key contributors in neurodegenerative diseases[23,24]. Given these diverse pharmacological activities, I3O holds promise as a therapeutic agent in treating various conditions, including cancer, inflammatory disorders, and neurodegenerative diseases.

In this context, I3O has garnered attention for its potential to alleviate the effects of male infertility from elevated temperatures. By inhibiting sEH, I3O may preserve EET levels, thereby reducing inflammation, oxidative stress, and vascular dysfunction, critical factors in reproductive health[25–27]. This study aimed to investigate the effects of I3O on heat-induced reductions in egg-hatching rates in *Drosophila* to assess its potential as a therapeutic agent. Additionally, this study explored the molecular interactions between I3O and sEH through docking and molecular dynamics (MD) simulations, providing a comprehensive understanding of the role of I3O in enhancing reproductive outcomes under stress conditions.

Materials and methods

Chemicals and reagents

I3O (I0404) and Bis–Tris buffer (B9754) were purchased from Sigma-Aldrich (St. Louis, MO). sEH (human, recombinant; Item No. 10011669), PHOME (Item No. 10009134), and AUDA (Item No. 10007927) were purchased from Cayman Chemical (Ann Arbor, MI).

Drosophila strain and culture

All *Drosophila* stocks were maintained on standard cornmeal molasses agar media at 25 °C and 40–60% humidity. The *w1118* strain, obtained from the Bloomington Drosophila Stock Center (BDSC, Bloomington, IN), was used to measure egg-hatching rates.

Analysis of Drosophila egg-hatching rate

To examine how temperature affects the reproductive capacity of *Drosophila*, eggs were collected from a newly prepared vial containing a food and test compound (I3O) mixture over six hours. These vials were then placed in an incubator at 27.5 °C, allowing

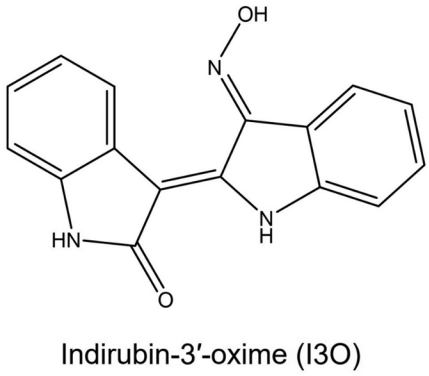

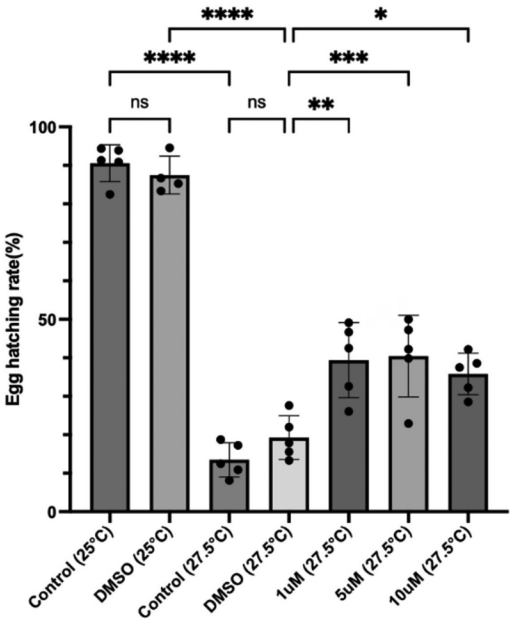

Figure 1. Indirubin-3′-oxime, and its impact on *Drosophila* egg-hatching rates. The mean ± SEM; *$p < 0.05$, **$p < 0.01$, ***$p < 0.001$, and ****$p < 0.0001$, followed by Tukey's post hoc test.

Table 1. Impact of I3O on *Drosophila* egg counts.

									I3O (27.5 °C)					
	Control (25 °C)		DMSO (25 °C)		Control (27.5 °C)		DMSO (27.5 °C)		1 μM		5 μM		10 μM	
Repeat	Egg	Hatched	Egg	Hatched	Egg	Hatched	Egg	Hatched	Egg	Hatched	Egg	Hatched	Egg	Hatched
1	49	46	60	52	86	7	122	19	119	31	109	25	31	10
2	46	42	55	52	56	7	30	4	61	26	28	14	70	27
3	137	113	48	40	80	15	100	22	114	56	91	43	80	30
4	53	50	34	29	46	5	28	5	60	28	45	19	49	14
5	22	20	–	–	139	24	29	8	43	14	113	45	83	35

the eggs to grow into adult flies. Male flies from this group were paired with virgin females grown at 25 °C with no exposure to any chemical. After mating, the flies were moved to grape agar plates, where they laid eggs overnight. The following day, the quantity of laid eggs was counted. The grape agar plates were incubated at 25 °C, and egg hatching was recorded over 24 h to assess fertility. Data on the number of hatched eggs and the hatching rate were then measured and analysed.

sEH inhibition assay

The sEH inhibitory activity was assessed using our established procedures[28,29]. Initially, 130 µL of sEH enzyme in Bis–Tris buffer (pH 7.0) containing 0.1% bovine serum albumin, along with 20 µL of test compound I3O diluted in DMSO, were combined in 96-well plates. Subsequently, 50 µL of the PHOME substrate was added to each well and incubated at 37 °C. Fluorescence measurements were taken over 40 min using a VICTOR Nivo microplate reader (PerkinElmer, Waltham, MA), with excitation and emission wavelengths set at 330 nm and 460 nm, respectively. AUDA was used as the positive control. The inhibitory activity was calculated using the equation:

$$\text{Inhibitory activity rate}\,(\%) = [1-(\Delta Inhibitor / \Delta Control)] \times 100\%$$

where $\Delta Inhibitor$ and $\Delta Control$ are the fluorescence values of the inhibitor and control, respectively, after 40 min. The IC_{50} values were determined using Microsoft Excel 365 (Redmond, WA).

Furthermore, two enzyme kinetic methods (Lineweaver–Burk and Dixon plots) were employed to evaluate the inhibition mode and calculate the inhibition constant (K_i) of I3O[30,31]. The results were analysed and presented using Microsoft Excel 365 (Redmond, WA).

Molecular docking

The molecular docking simulations were conducted using AutoDock Vina 1.1.2 (Scripps Research Institute, La Jolla, CA)[32], according to the developer's protocol[33]. The 3D structure of human sEH (PDB ID: 3ANS) with a resolution of 1.98 Å was obtained from the Protein Data Bank. The protein was prepared using BIOVIA Discovery Studio Visualizer v21 (Dassault Systèmes, San Francisco, CA). The 3D model of I3O was built and energy-minimised using Spartan'24 (Wavefunction, Irvine, CA). The sEH and I3O structures were then converted to PDBQT format using AutoDockTools 1.5.6. A grid box encompassing the entire surface of the target protein was established for the docking simulations. Finally, the 2D and 3D docking interactions were analysed and visualised using Discovery Studio Visualizer.

Table 2. Impact of I3O on *Drosophila* egg-hatching rates (% hatched).

Repeat	Control (25 °C)	DMSO (25 °C)	Control (27.5 °C)	DMSO (27.5 °C)	I3O (27.5 °C) 1 µM	I3O (27.5 °C) 5 µM	I3O (27.5 °C) 10 µM
1	93.88%	86.67%	8.14%	15.57%	26.05%	22.94%	32.26%
2	91.30%	94.55%	12.50%	13.33%	42.62%	50.00%	38.57%
3	82.48%	83.33%	18.75%	22.00%	49.12%	47.25%	37.50%
4	94.34%	85.29%	10.87%	17.86%	46.67%	42.22%	28.57%
5	90.91%	–	17.27%	27.59%	32.56%	39.82%	42.17%

Table 3. sEH inhibition by I3O.

Compound	IC_{50}	Inhibition type[a]	K_i (µM)[b]
I3O	59.74 ± 0.41 µM	Non-competitive	78.88
AUDA[c]	17.79 ± 0.08 nM	–	–

(–) Not tested.
[a]Determined using the Lineweaver–Burk plot.
[b]Determined using the Dixon plot.
[c]Positive control.

Molecular dynamics simulations

MD simulations were conducted using GROMACS 2022.1, based on our previous procedures[28,29]. The system was set up using the CHARMM-GUI web platform, with the CHARMM36 force field applied. Periodic boundary conditions were implemented using a TIP3P explicit solvation model, with box dimensions of 7.39 × 7.39 × 7.39 $Å^3$. Na^+ and/or Cl^- ions were added to the system to ensure neutrality and equilibrium. Then, the complexes underwent energy minimisation using a 10 kJ/mol maximum force threshold. This was followed by a 100 ns MD simulation, starting with NVT equilibration at 300 K, and transitioning to NPT ensemble relaxation at 1 atm.

During the equilibration phase, position restraints were applied to the heavy atoms of the protein to maintain their positions and stabilise the structure. No elastic constant restraints were applied to the ligand, allowing it to move freely and explore the binding pocket. The simulation trajectory data were then analysed and visualised using PyMOL 2.5.4 (Schrödinger) and Grace software (https://plasma-gate.weizmann.ac.il/Grace/). The molecular surface area analysis was also identified using the SurfinMD program (http://lmdm.biof.ufrj.br/en/software/)[34].

Statistical analysis

The results are presented as the mean ± standard error of the mean (SEM) from at least three independent experiments. Statistical significance was determined at $p < 0.05$ using one-way ANOVA and Duncan's multiple-range test.

Results and discussion

Effect of I3O on heat-induced reductions in Drosophila egg-hatching rates

In this study, the potential of the compound I3O to alleviate the effects of elevated temperature on male infertility was investigated, with egg-hatching rates in *Drosophila* used as a key indicator (Figure 1, Tables 1 and 2). Normally, male infertility increases under heat stress by reducing egg viability[4,35]. High egg-hatching rates, ranging from 82.48% to 94.34%, were observed in the control group at 25 °C, reflecting normal male fertility under optimal temperature conditions. However, when the temperature was increased to 27.5 °C, a significant decline in hatching rates was recorded in the control group, with values ranging between 8.14% and 18.75%. This decline confirms elevated temperatures negatively affect male fertility by reducing egg viability.

In the DMSO-treated group at 27.5 °C, hatching rates remained low, ranging from 13.33% to 27.59%, indicating that DMSO alone did not mitigate the impact of heat stress. DMSO was used as a control because I3O was dissolved in it for administration. This ensured that any observed effects in the experimental groups could be attributed to I3O and not to the solvent itself. Additionally,

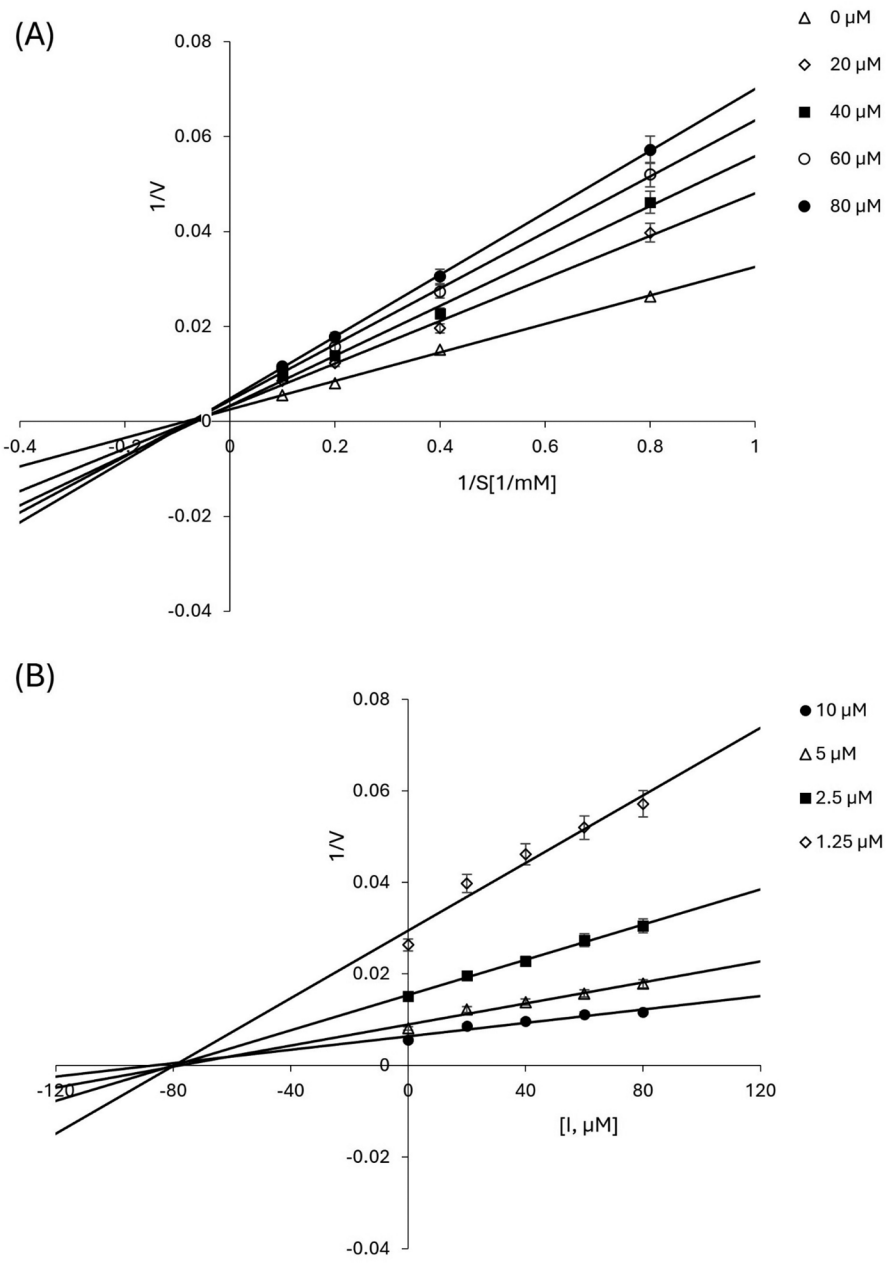

Figure 2. The Lineweaver–Burk plot (A) and Dixon plot (B) for the sEH inhibition by I3O.

DMSO was present in all I3O-treated groups to maintain consistency in the experimental conditions.

An improvement in hatching rates was observed with dietary supplementation of I3O. At a concentration of 1 μM, hatching rates increased between 26.05% and 49.12%, suggesting that I3O can partially restore fertility in males exposed to elevated temperatures. The improvement was more pronounced at 5 μM, where hatching rates ranged from 22.94% to 50.00%, and at the highest concentration of 10 μM, hatching rates reached 28.57–42.17%. These findings indicate that the negative effects of elevated temperatures on male fertility in *Drosophila* can be mitigated by I3O supplementation. Moreover, the increase in hatching rates demonstrates that I3O has the potential as a protective agent against temperature-induced male infertility. Although the hatching rates at 10 μM did not fully return to the levels observed at 25 °C, a significant improvement was demonstrated compared to the DMSO-treated and high-temperature control groups.

Table 4. I3O binding affinity and binding interactions with sEH.

Compound	Binding affinity (kcal/mol)	Hydrogen bonds	van der Waals interactions	Hydrophobic interactions
I3O	−9.2	Ser415 (2.44 Å)	Val380	Tyr383 (π–π T-shaped, 5.19 Å)
		Leu417 (3.06 Å)	Leu408	Phe497 (π–π T-shaped, 5.31 Å)
		Trp525 (2.31 Å)	Ser418	Met419 (π–alkyl, 5.03 Å)
			Tyr466	Val498 (π–alkyl, 4.56 Å)

sEH inhibitory effects of I3O

In addition to its impact on egg-hatching rates, the ability of I3O to inhibit sEH was also investigated. sEH is an enzyme involved in the metabolism of EETs, which play a role in inflammation, vascular function, and hormonal regulation[36–38]. Since

EETs are crucial for maintaining reproductive health, sEH inhibition may help address reproductive issues such as male infertility by reducing inflammation and improving blood flow. The sEH inhibition by I3O was assessed, revealing a potential IC_{50} value of 59.74 ± 0.41 μM (Table 3). Enzyme kinetics experiments were conducted using Lineweaver–Burk[30] and Dixon plots[31] to determine the mode of inhibition by I3O. Non-competitive inhibition is characterised by straight lines intersecting at a common point on the *x*-axis in a Lineweaver–Burk plot, while competitive inhibition is indicated by lines intersecting at a common point on the *y*-axis. The Lineweaver–Burk plot was generated using substrate concentrations of 2.5, 5, 10, and 20 μM and I3O concentrations of 0, 20, 40, 60, and 80 μM. These results indicated that I3O is a non-competitive sEH inhibitor (Figure 2(A)). The K_i value of I3O, which represents the concentration required to achieve half-maximal sEH inhibition, was determined using the Dixon plot and confirmed a K_i value of 78.88 μM (Figure 2(B)). The enzyme kinetics results suggest that I3O binds to a site on

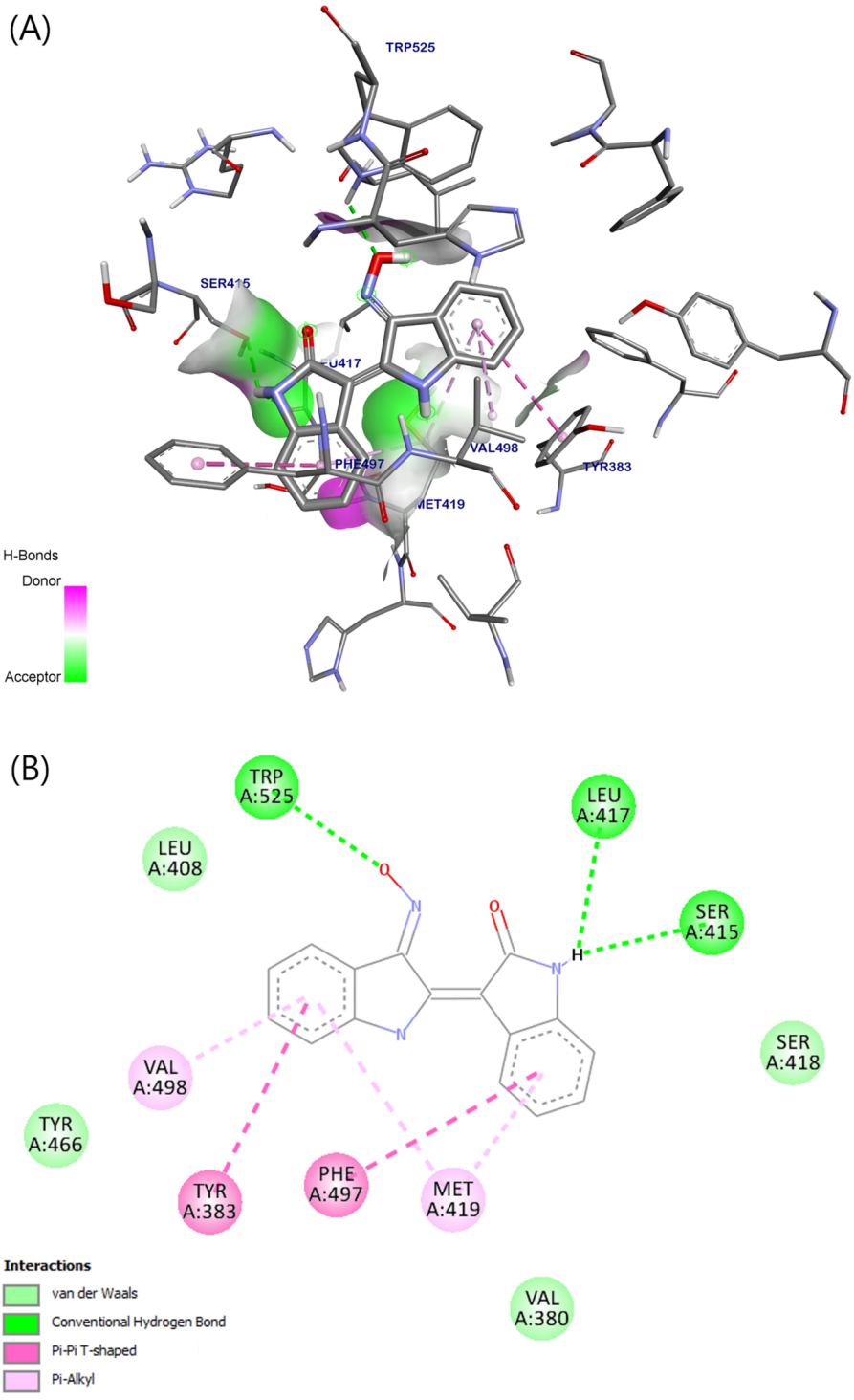

Figure 3. Docking pose (A) and interactions diagram (B) results of I3O with sEH. Green lines: hydrogen bonds; light green: van der Waals interactions; dark pink: π–π T-shaped interactions; light pink: π–alkyl interactions.

the enzyme that is distinct from the active site, thereby reducing enzyme activity without directly competing with the substrate.

For comparison, AUDA, a well-known sEH inhibitor[39], was used as the positive control and showed a significantly lower IC_{50} value of 17.79 ± 0.08 nM. This stark difference highlights that while I3O exhibits sEH inhibitory activity, it is less potent than AUDA. However, the non-competitive nature of the I3O-induced inhibition could offer unique advantages in therapeutic contexts where partial inhibition or modulation of sEH activity is desirable.

Molecular docking

In this study, docking simulations were conducted using AutoDock Vina 1.1.2 to explore the significant interactions between I3O and human sEH. The human sEH enzyme consists of two independent functional domains: the N-terminal domain, which exhibits phosphatase activity, and the C-terminal domain, which possesses hydrolase activity[40,41]. Structurally, the C-terminal domain contains an L-shaped pocket, buried within the protein core. This pocket is predominantly hydrophobic, accommodating the hydrophobic nature of the lipid substrates. The catalytic triad, comprising Asp335, Asp496, and His524, is centrally located within this pocket, flanked by two stabilising residues, Tyr383 and Tyr466[42,43]. These structural features are crucial for the enzyme's catalytic efficiency and substrate specificity.

Beyond the catalytic site, potential allosteric sites were identified through a combination of literature review and structural analysis. Previous studies have highlighted regions near residues Cys423 and Cys522 as allosteric sites[41,44], which can modulate enzyme activity through non-competitive inhibition. These sites were characterised by examining the structural dynamics of the enzyme and the spatial arrangement of these residues, indicating their potential role in facilitating conformational changes upon inhibitor binding. This suggests that inhibitors targeting these sites could reduce the catalytic function of the enzyme, making them promising therapeutic targets.

To ensure that the docking process was comprehensive and unbiased, the grid box was designed to cover the entire enzyme surface. This allowed for exploration of both the catalytic and allosteric sites. The docking results revealed that the majority of high-affinity binding poses for I3O localised consistently to the allosteric site, particularly near residues Cys423 and Cys522.

The binding affinity of I3O to the sEH enzyme was determined to be −9.2 kcal/mol, indicating a strong interaction (Table 4). The docking simulations revealed that I3O forms multiple hydrogen bonds with critical residues, including Ser415, Leu417, and Trp525, in the allosteric site via amine groups (Figure 3). The compound also engages in van der Waals interactions with several residues, such as Val380, Leu408, Ser418, and Tyr466. Additionally, the benzene rings of I3O participate in specific hydrophobic interactions with Tyr383 and Phe497 through π–π T-shaped interactions, and Met419 and Val498 through π–alkyl interactions. Notably, the linkages with the stabilising residues Tyr383 and Tyr466 observed in the docking poses of I3O with sEH suggest that these interactions may further enhance the binding stability of I3O within the enzyme's allosteric site, thereby increasing its overall binding affinity.

Molecular dynamics

In addition to docking simulations, MD simulations were performed for 100 ns using GROMACS 2022.1 to assess the conformational stability of the sEH–I3O complex and its variants. These simulations provided deeper insights into the dynamic behaviour of the enzyme-compound complex, complementing the docking results and offering a more comprehensive understanding of the interactions and stability of the complex over time[45].

The MD simulations demonstrated the stability of the sEH–I3O complex throughout the 100 ns simulation period. As shown in Figure 4, the potential and total energy plots exhibited minor fluctuations, indicating that the system reached equilibrium early in the simulation and maintained stability afterward. The average

Energy	Average	Err.Est.	RMSD	Tot-Drift	
Potential	-516000	54	824.198	-344.265	(kJ/mol)

Energy	Average	Err.Est.	RMSD	Tot-Drift	
Total Energy	-410109	54	1105.72	-338.82	(kJ/mol)

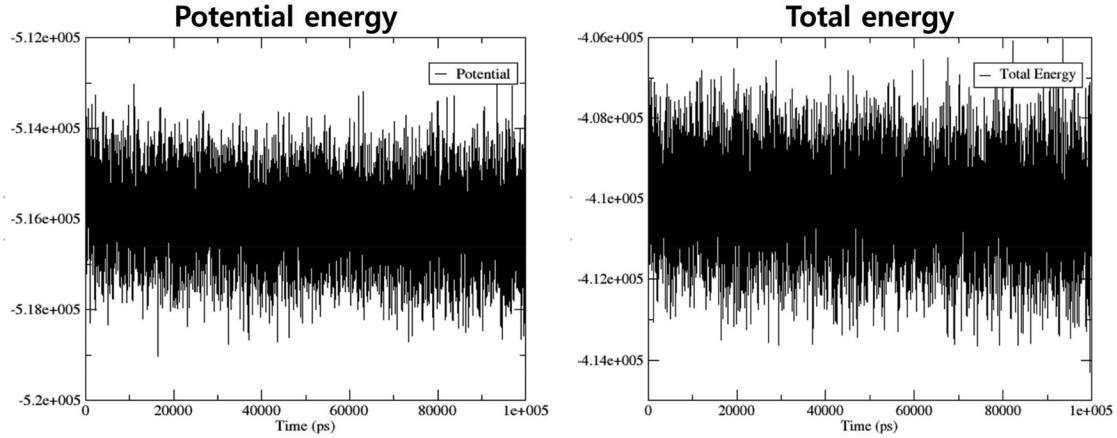

Figure 4. Energy profiles, potential, and total energy plots of the molecular dynamics simulation for I3O with sEH.

potential energy was approximately −516 000 kJ/mol, while the average total energy was around −410 109 kJ/mol (Figure 4). To further evaluate the stability and conformational dynamics of the sEH–I3O complex, root mean square deviation (RMSD) and root mean square fluctuation (RMSF) analyses were conducted. The RMSD plot for the protein backbone (Figure 5(A)) showed that the system fluctuated sharply from 0.13 to 0.21 nm during the initial 10 ns of equilibrium, gradually increased from 0.21 to 0.25 nm over the next 30 ns, and achieved equilibrium within the first 50 ns. The RMSD values then remained stable around 0.25 nm for the remainder of the 100 ns simulation, indicating that the overall structure of the sEH enzyme was well-maintained and further confirming the stability of the sEH–I3O complex. The RMSF plot (Figure 5(B)) provided insights into the flexibility of individual residues within the protein. Most residues exhibited low fluctuations, with RMSF values generally below 0.2 nm, indicating a stable structure. However, higher fluctuations were observed in certain regions, particularly in the N-terminus, with RMSF values reaching approximately 0.35 nm. These regions may be more flexible or involved in binding interactions. However, these regions are located far from the I3O binding site with sEH, suggesting that these fluctuations do not affect the binding interactions between I3O and the sEH enzyme.

Hydrogen bond analysis was conducted to evaluate interactions between I3O and the sEH enzyme. The analysis involved a system with 4998 protein atoms and 32 ligand atoms, identifying 440 donors and 887 acceptors. During the 100 ns simulation, the number of hydrogen bonds fluctuated between 1 and 4 (Figure 6(A)), with a

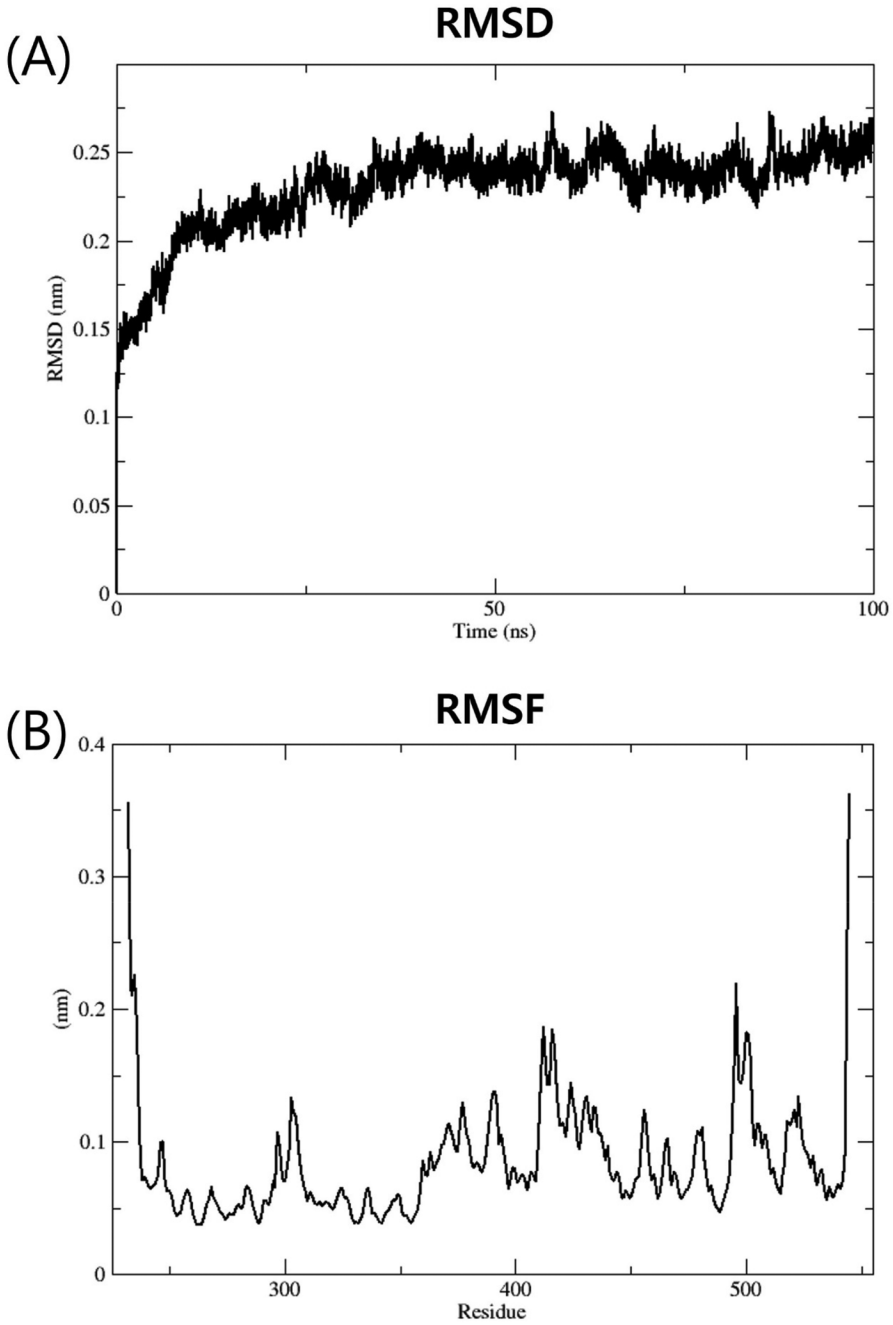

Figure 5. Molecular dynamics simulations. Root mean square deviation (RMSD, A) and root mean square fluctuation (RMSF, B) plots for the binding of I3O with sEH.

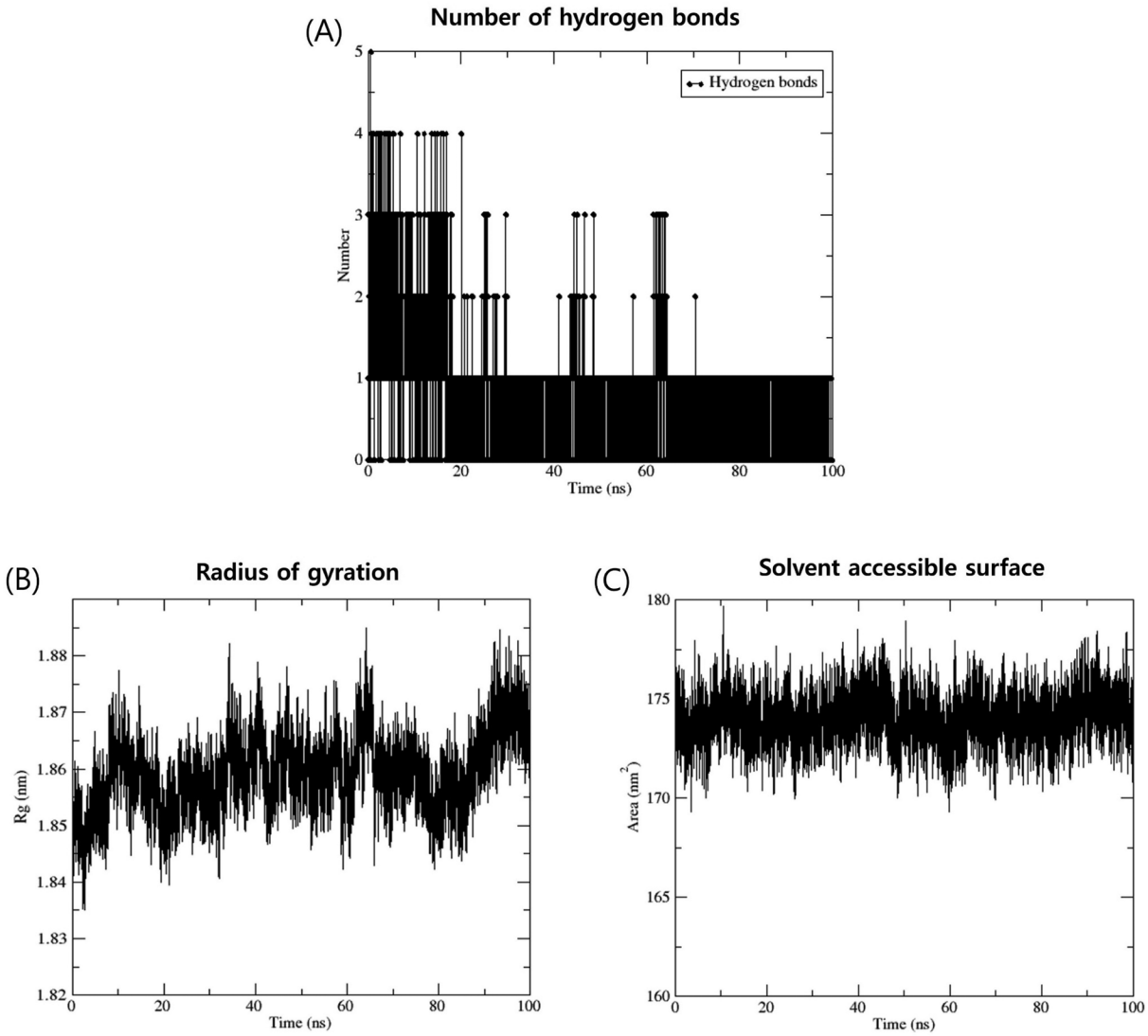

Figure 6. Molecular dynamics simulations. Number of hydrogen bonds (A), radius of gyration (B), and solvent accessible surface area (C) plots for the binding of I3O with sEH.

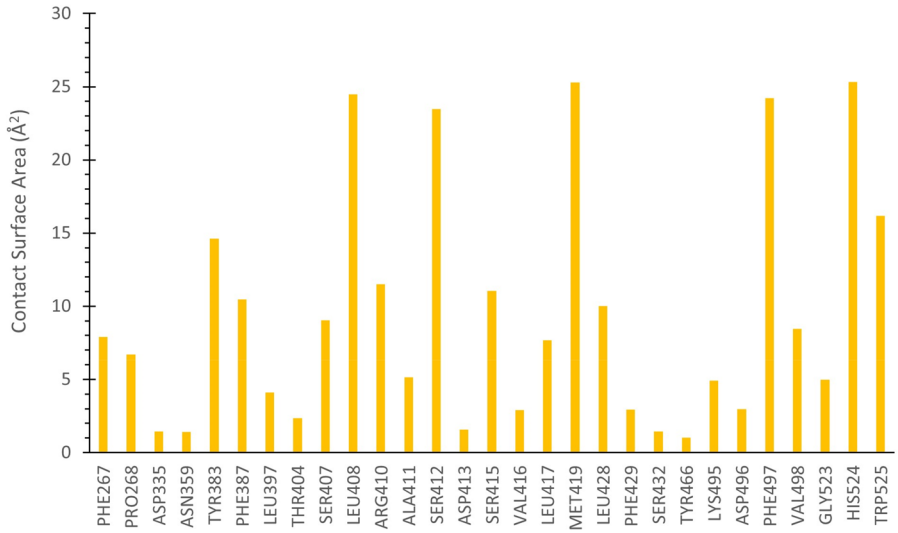

Figure 7. SurfinMD calculated the surface molecular area of specific interactions for binding I3O with sEH.

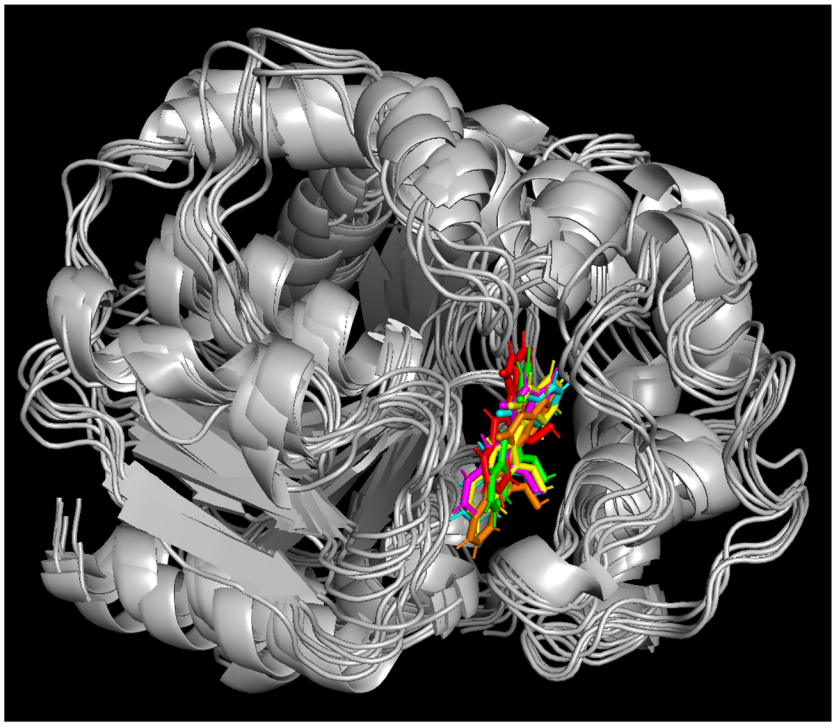

Figure 8. Superposition of I3O with sEH was recorded every 20 ns throughout the 100 ns molecular dynamics simulation. Red: 0 ns; green: 20 ns; yellow: 40 ns; magenta: 60 ns; cyan: 80 ns; orange: 100 ns.

total of 25 distinct hydrogen bonds identified. The effective number of unique hydrogen bonds consistently maintained throughout the simulation was 22. The average occupancy was approximately 84.6%, indicating that these interactions were frequently maintained during the simulation. This high occupancy reflects a stable interaction between I3O and sEH, suggesting that the binding significantly contributes to the structural stability of the complex.

The radius of gyration (Rg) of the sEH–I3O complex was approximately 1.855 nm (Figure 6(B)), indicating the compactness of the protein structure during the simulation[46]. A stable Rg value throughout the 100 ns simulation suggests no significant structural changes and that the protein maintained its overall shape and compactness. This stability is crucial as it indicates that I3O binding does not cause major unfolding or structural disruption of the sEH enzyme.

The solvent-accessible surface area (SASA) was measured at around 174 nm^2 (Figure 6(C)), reflecting the extent of the protein surface accessible to the solvent[47]. Additionally, contact surface area analysis of specific interactions involving sEH and I3O, conducted using the SurfinMD program (Figure 7), revealed interactions with residues Tyr383 (14.62 $Å^2$), Leu408 (24.47 $Å^2$), Met419 (25.28 $Å^2$), Phe497 (24.22 $Å^2$), and Trp525 (16.16 $Å^2$). Interactions with Ser412 (23.46 $Å^2$) and His524 (25.32 $Å^2$) were also observed, strongly supporting the results of the molecular docking simulations.

Figure 8 presents the superposition of I3O within the sEH binding site throughout the 100 ns MD trajectory. No significant fluctuations were observed, indicating consistent binding and further supporting the conclusion that I3O binding did not induce large conformational shifts within the sEH enzyme, thereby maintaining the structural integrity of the protein throughout the simulation.

Conclusions

This study highlights the potential of I3O as a protective agent against temperature-induced male infertility. The compound demonstrated an ability to improve egg-hatching rates in *Drosophila* under heat stress, indicating its efficacy in partially restoring male fertility. Furthermore, I3O inhibited sEH through non-competitive inhibition, suggesting that it binds to an allosteric site on the enzyme. Molecular docking and MD simulations revealed strong interactions between I3O and critical residues within the sEH enzyme, further supporting its inhibitory role and stability within the allosteric site of the enzyme.

Although I3O is less potent than known sEH inhibitors such as AUDA, its non-competitive inhibition and ability to enhance binding stability offer unique therapeutic advantages, particularly when partial enzyme inhibition is desirable. The results of this study provide valuable insights into the potential mechanisms through which I3O may exert its protective effects. However, the exact mechanism of action in male *Drosophila* has not yet been determined, and it remains unclear whether I3O inhibits sEH specifically during spermatogenesis. Further research is needed to explore this mechanism and determine if sEH homologs are expressed in the *Drosophila* testis, based on tissue-specific expression data. These findings hold promise for future investigations into the potential use of I3O as a therapeutic agent for male infertility and other conditions associated with elevated sEH activity.

Author contributions

Nguyen Viet Phong and Hyo-Sung Kim: investigation, formal analysis, data curation, and writing – original draft. Yan Zhao: investigation. Eunbyul Yeom and Seo Young Yang: conceptualisation, methodology, writing – review and editing, and supervision.

Ethics statement

This study did not involve human participants, human samples, or live vertebrate animals. The research was conducted using *Drosophila melanogaster* (fruit flies), which are invertebrates.

Therefore, the study does not fall under the guidelines of the Declaration of Helsinki or the ARRIVE Guidelines 2.0.

Disclosure statement

The authors report no conflicts of interest.

Funding

This research was supported by the National Research Foundation of Korea (NRF) funded by the Korea Government (MSIT) (No. NRF – 2022R1C1C1004636 and 2022R1C1C100636712) and Global – Learning & Academic Research Institution for Master's·PhD Students, and Postdocs (LAMP) Program of the National Research Foundation of Korea (NRF) grant funded by the Ministry of Education (No. RS-2023-00301914).

ORCID

Nguyen Viet Phong http://orcid.org/0000-0003-1715-4455
Seo Young Yang http://orcid.org/0000-0002-5248-1374

Data availability statement

The datasets presented in the current study are available from the corresponding author upon reasonable request.

References

1. Kumar N, Singh AK. Impact of environmental factors on human semen quality and male fertility: a narrative review. Environ Sci Eur. 2022;34(1):6.
2. Durairajanayagam D. Lifestyle causes of male infertility. Arab J Urol. 2018;16(1):10–20.
3. Okonofua FE, Ntoimo LFC, Omonkhua A, Ayodeji O, Olafusi C, Unuabonah E, Ohenhen V. Causes and risk factors for male infertility: a scoping review of published studies. Int J Gen Med. 2022;15:5985–5997.
4. Canal Domenech B, Fricke C. Recovery from heat-induced infertility—a study of reproductive tissue responses and fitness consequences in male *Drosophila melanogaster*. Ecol Evol. 2022;12(12):e9563.
5. Gärtner SMK, Hundertmark T, Nolte H, Theofel I, Eren-Ghiani Z, Tetzner C, Duchow TB, Rathke C, Krüger M, Renkawitz-Pohl R. Stage-specific testes proteomics of *Drosophila melanogaster* identifies essential proteins for male fertility. Eur J Cell Biol. 2019;98(2–4):103–115.
6. Gandara ACP, Drummond-Barbosa D. Chronic exposure to warm temperature causes low sperm abundance and quality in *Drosophila melanogaster*. Sci Rep. 2023;13(1):12331.
7. Zhang J, Luo J, Chen J, Dai J, Montell C. The role of Y chromosome genes in male fertility in *Drosophila melanogaster*. Genetics. 2020;215(3):623–633.
8. Ritchie C, Ko EY. Oxidative stress in the pathophysiology of male infertility. Andrologia. 2021;53(1):e13581.
9. Kim JH, Morgan AMA, Tai BH, Van DT, Cuong NM, Kim YH. Inhibition of soluble epoxide hydrolase activity by compounds isolated from the aerial parts of *Glycosmis stenocarpa*. J Enzyme Inhib Med Chem. 2016;31(4):640–644.
10. Kim HS, Moon S-J, Lee SE, Hwang GW, Yoo HJ, Song JW. The arachidonic acid metabolite 11,12-epoxyeicosatrienoic acid alleviates pulmonary fibrosis. Exp Mol Med. 2021;53(5):864–874.
11. Swardfager W, Hennebelle M, Yu D, Hammock BD, Levitt AJ, Hashimoto K, Taha AY. Metabolic/inflammatory/vascular comorbidity in psychiatric disorders; soluble epoxide hydrolase (sEH) as a possible new target. Neurosci Biobehav Rev. 2018;87:56–66.
12. Szczuko M, Kikut J, Komorniak N, Bilicki J, Celewicz Z, Ziętek M. The role of arachidonic and linoleic acid derivatives in pathological pregnancies and the human reproduction process. Int J Mol Sci. 2020;21(24):9628.
13. Kikut J, Komorniak N, Ziętek M, Palma J, Szczuko M. Inflammation with the participation of arachidonic (AA) and linoleic acid (LA) derivatives (HETEs and HODEs) is necessary in the course of a normal reproductive cycle and pregnancy. J Reprod Immunol. 2020;141:103177.
14. Hu J, Sisignano M, Brecht R, Perumal N, Angioni C, Bibli I-S, Fisslthaler B, Kleinert H, Pfeiffer N, Fleming I, et al. Cyp2c44 epoxygenase-derived epoxyeicosatrienoic acids in vascular smooth muscle cells elicit vasoconstriction of the murine ophthalmic artery. Sci Rep. 2021;11(1):18764.
15. Malacarne PF, Bezzenberger J, Lopez M, Warwick T, Müller N, Brandes RP, Rezende F. Epoxyeicosatrienoic acid and prostanoid crosstalk at the receptor and intracellular signaling levels to maintain vascular tone. Int J Mol Sci. 2022;23(11):5939.
16. Cuong NM, Tai BH, Hoan DH, Long PQ, Choi E-M, Kim YH. Synthesis and anti-osteoporosis potential of two new indirubin-3′-oxime derivatives. J Korean Soc Appl Biol Chem. 2009;53(1):22–26.
17. Cuong NM, Tai BH, Hoan DH, Huong TT, Kim YH, Hyun J-H, Kang H-K. Inhibitory effects of indirubin derivatives on the growth of HL-60 leukemia cells. Nat Prod Commun. 2010;5(1):103–106.
18. Dan NT, Quang HD, Van Truong V, Huu Nghi D, Cuong NM, Cuong TD, Toan TQ, Bach LG, Anh NHT, Mai NT, et al. Design, synthesis, structure, in vitro cytotoxic activity evaluation and docking studies on target enzyme GSK-3β of new indirubin-3′-oxime derivatives. Sci Rep. 2020;10(1):11429.
19. Yu J, Zheng J, Lin J, Jin L, Yu R, Mak S, Hu S, Sun H, Wu X, Zhang Z, et al. Indirubin-3-oxime prevents H_2O_2-induced neuronal apoptosis via concurrently inhibiting GSK3β and the ERK pathway. Cell Mol Neurobiol. 2017;37(4):655–664.
20. Ichimaru Y, Sano M, Kajiwara I, Tobe T, Yoshioka H, Hayashi K, Ijichi H, Miyairi S. Indirubin 3′-oxime inhibits migration, invasion, and metastasis in vivo in mice bearing spontaneously occurring pancreatic cancer via blocking the RAF/ERK, AKT, and SAPK/JNK pathways. Transl Oncol. 2019;12(12):1574–1582.
21. Nguyen TD, Le TMD. Development of a novel indirubin derivative with enhanced anticancer properties: synthesis, in vitro, and in vivo evaluation. Chem Pap. 2024;78(4):2469–2478.
22. Tanaka T, Ohashi S, Saito H, Wada T, Aoyama T, Ichimaru Y, Miyairi S, Kobayashi S. Indirubin 3′-oxime inhibits anticancer agent-induced YB-1 nuclear translocation in HepG2 human hepatocellular carcinoma cells. Biochem Biophys Res Commun. 2018;496(1):7–11.
23. Jung H-J, Nam KN, Son M-S, Kang H, Hong J-W, Kim JW, Lee EH. Indirubin-3′-oxime inhibits inflammatory activation of rat brain microglia. Neurosci Lett. 2011;487(2):139–143.
24. Zhang S, Zhang Y, Xu L, Lin X, Lu J, Di Q, Shi J, Xu J. Indirubin-3′-monoxime inhibits β-amyloid-induced neurotoxicity in neuroblastoma SH-SY5Y cells. Neurosci Lett. 2009;450(2):142–146.

25. Turnell BR, Kumpitsch L, Reinhardt K. Production and scavenging of reactive oxygen species both affect reproductive success in male and female *Drosophila melanogaster*. Biogerontology. 2021;22(4):379–396.
26. Okada K, Blount JD, Sharma MD, Snook RR, Hosken DJ. Male attractiveness, fertility and susceptibility to oxidative stress are influenced by inbreeding in *Drosophila simulans*. J Evol Biol. 2011;24(2):363–371.
27. Nguyen-Powanda P, Robaire B. Oxidative stress and reproductive function in the aging male. Biology. 2020;9(9):282.
28. Phong NV, Van Cong P, Min BS, Yang SY, Kim JA. Inhibitory effects of phenylpropanoids and lignans isolated from the bark of *Cinnamomum cassia* L. on soluble epoxide hydrolase: spectroscopic, kinetic, molecular docking, and molecular dynamics studies. J Mol Struct. 2024;1301:137376.
29. Phong NV, Thao NP, Vinh LB, Luyen BTT, Minh CV, Yang SY. Inhibition of soluble epoxide hydrolase by cembranoid diterpenes from soft coral *Sinularia maxima*: enzyme kinetics, molecular docking, and molecular dynamics. Mar Drugs. 2024;22(8):373.
30. Lineweaver H, Burk D. The determination of enzyme dissociation constants. J Am Chem Soc. 1934;56(3):658–666.
31. Burlingham BT, Widlanski TS. An intuitive look at the relationship of Ki and IC_{50}: a more general use for the Dixon plot. J Chem Educ. 2003;80(2):214.
32. Trott O, Olson AJ. AutoDock Vina: improving the speed and accuracy of docking with a new scoring function, efficient optimization, and multithreading. J Comput Chem. 2010;31(2):455–461.
33. Forli S, Huey R, Pique ME, Sanner MF, Goodsell DS, Olson AJ. Computational protein–ligand docking and virtual drug screening with the AutoDock suite. Nat Protoc. 2016;11(5):905–919.
34. Silva RC, Freitas HF, Campos JM, Kimani NM, Silva CHTP, Borges RS, Pita SSR, Santos CBR. Natural products-based drug design against SARS-CoV-2 Mpro 3CLpro. Int J Mol Sci. 2021;22(21):11739.
35. Phong NV, Kim H-S, Park H-J, Yeom E, Yang SY. Assessing the efficacy of acanthoic acid isolated from *Acanthopanax koreanum* Nakai in male infertility: an in vivo and in silico approach. Curr Issues Mol Biol. 2024;46(7):7411–7429.
36. Huang A, Sun D. Sexually dimorphic regulation of EET synthesis and metabolism: roles of estrogen. Front Pharmacol. 2018;9:1222.
37. Lee AR, Pechenino AS, Dong H, Hammock BD, Knowlton AA. Aging, estrogen loss and epoxyeicosatrienoic acids (EETs). PLOS One. 2013;8(8):e70719.
38. Seubert JM, Zeldin DC, Nithipatikom K, Gross GJ. Role of epoxyeicosatrienoic acids in protecting the myocardium following ischemia/reperfusion injury. Prostaglandins Other Lipid Mediat. 2007;82(1–4):50–59.
39. Duan L, Song L, Qiu C, Li J. Effect of the sEH inhibitor AUDA on arachidonic acid metabolism and NF-κB signaling of rats with postpartum depression-like behavior. J Neuroimmunol. 2023;385:578250.
40. Bzówka M, Mitusińska K, Hopko K, Góra A. Computational insights into the known inhibitors of human soluble epoxide hydrolase. Drug Discov Today. 2021;26(8):1914–1921.
41. Oanh VT, Phong NV, Min BS, Yang SY, Kim JA. Insights into the inhibitory activities of neolignans and diarylnonanoid derivatives from nutmeg (*Myristica fragrans* Houtt.) seeds on soluble epoxide hydrolase using in vitro and in silico approaches. J Enzyme Inhib Med Chem. 2023;38(1):2251099.
42. Gurung AB, Mayengbam B, Bhattacharjee A. Discovery of novel drug candidates for inhibition of soluble epoxide hydrolase of arachidonic acid cascade pathway implicated in atherosclerosis. Comput Biol Chem. 2018;74:1–11.
43. Dötsch L, Davies C, Hennes E, Schönfeld J, Kumar A, Guita CDCL, Ehrler JHM, Hiesinger K, Thavam S, Janning P, et al. Discovery of the sEH inhibitor epoxykynin as a potent kynurenine pathway modulator. J Med Chem. 2024;67(6):4691–4706.
44. Qiu Q, Abis G, Mattingly-Peck F, Lynham S, Fraternali F, Conte MR. Allosteric regulation of the soluble epoxide hydrolase by nitro fatty acids: a combined experimental and computational approach. J Mol Biol. 2022;434(17):167600.
45. Jo AR, Kim JH, Yan X-T, Yang SY, Kim YH. Soluble epoxide hydrolase inhibitory components from *Rheum undulatum* and in silico approach. J Enzyme Inhib Med Chem. 2016;31(Suppl. 2):70–78.
46. Lobanov MY, Bogatyreva NS, Galzitskaya OV. Radius of gyration as an indicator of protein structure compactness. Mol Biol. 2008;42(4):623–628.
47. Ali Ausaf S, Hassan Imtaiyaz M, Islam A, Ahmad F. A review of methods available to estimate solvent-accessible surface areas of soluble proteins in the folded and unfolded states. Curr Protein Pept Sci. 2014;15(5):456–476.